Provided for non-commercial research and education use.
Not for reproduction, distribution or commercial use.

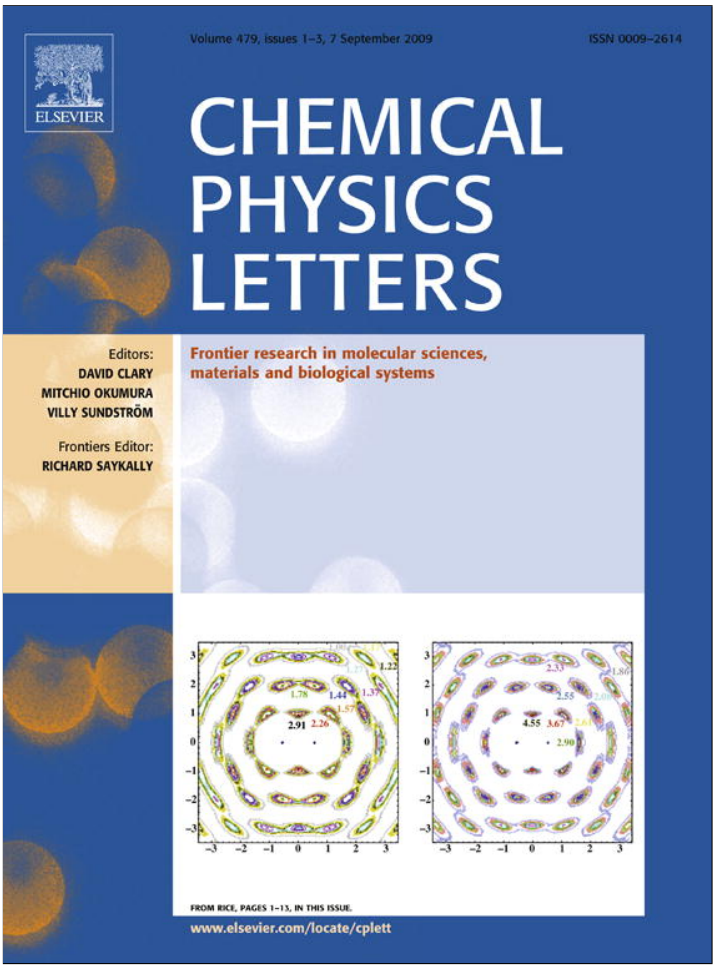

This article appeared in a journal published by Elsevier. The attached copy is furnished to the author for internal non-commercial research and education use, including for instruction at the authors institution and sharing with colleagues.

Other uses, including reproduction and distribution, or selling or licensing copies, or posting to personal, institutional or third party websites are prohibited.

In most cases authors are permitted to post their version of the article (e.g. in Word or Tex form) to their personal website or institutional repository. Authors requiring further information regarding Elsevier's archiving and manuscript policies are encouraged to visit:

http://www.elsevier.com/copyright

Author's personal copy

Chemical Physics Letters 479 (2009) 105–108

Contents lists available at ScienceDirect

Chemical Physics Letters

journal homepage: www.elsevier.com/locate/cplett

Kelvin Probe Force Microscopy study on hybrid P3HT:titanium dioxide nanorod materials

Tsung-Wei Zeng, Fang-Chi Hsu, Yu-Chieh Tu, Tsung-Han Lin, Wei-Fang Su *

Department of Materials Science and Engineering, National Taiwan University, Taipei 106, Taiwan

ARTICLE INFO

Article history:
Received 31 May 2009
In final form 31 July 2009
Available online 3 August 2009

ABSTRACT

We present a Kelvin Probe Force Microscopy (KPFM) study on the topography combined with surface potential of hybrid poly(3-hexylthiophene)(P3HT):TiO_2 nanorod materials in dark and under illumination. The hybrid materials with fine and coarse phase separation are displayed. The photo-induced electron accumulation on surface is pronounced under high loading TiO_2 nanorod in the blend. Large surface roughness, large surface height difference and potential variation in the hybrid P3HT:TiO_2 nanorod are present with high content TiO_2. Additionally, the incorporating a TiO_2 nanorod layer on the surface of hybrid layer to facilitate collecting the electron and blocking the hole is investigated.

© 2009 Elsevier B.V. All rights reserved.

1. Introduction

A variety of hybrid materials of conjugated polymer:inorganic nanocrystals are of great interest for efficient, low cost and large area polymer photovoltaic cells [1–3]. For efficient polymer:inorganic bulk heterojunction solar cells, the construction of nanodomain of each component for effective charge separation and high quality percolation pathways for the photo-generated electron and hole transporting from the hetero-interface to the respective charge collection electrodes are important factors [4].

Recently, the KPFM has been applied to resolve the degree and dimension of the phase separation in polymer bulk heterojunction [5–7]. The KPFM is allowed to map the structural and electronic properties of film surface of conjugated polymer based photovoltaic materials. The KPFM uses a non-contact atomic force microscopy tip with a conductive coating to measure the difference between the tip potential and the local surface potential [8] with a lateral and potential distribution below 70 nm and 10 mV. In addition, Kelvin probe measurements can be applied to study the charge carrier generation and electron blocking at inter-layers in polymer solar cells [9].

In the polymer bulk heterojunction solar cell, the hetero-interface and percolation networks remains highly sensitive to fabrication parameters, and the morphological defects are common. The KPFM is applied to exploit the presence of charge percolation paths and morphological defects within the bulk heterojunction facilitating one to gain deeper insight for the improvement of solar cell performance [10]. Previous KPFM studies on MDMO-PPV:PCBM films has demonstrated clear differences in the photovoltaic properties for the films with different morphologies, the result indicates the lower photocurrent in samples cast from toluene is due to hindered electron transporting to the cathode [5,11].

Performance of polymer:inorganic heterojunction solar cell is extremely sensitive to fabrication parameters. Among the key factors for the construction of hybrid, the content of nanocrystal is quite critical in determining the hetero-interface for exciton dissociation and percolated paths for charge transport in solar cells of MDMO-PPV:ZnO nanoparticle [2], P3HT:TiO_2 nanoparticle [12] and P3HT:TiO_2 nanorod [13]. According to Chang et al. [13], the optimized power conversion efficiency of the P3HT:TiO_2 nanorod hybrid solar cells consists of approximately 50 wt.% of TiO_2 nanorods. In this study, we resolve the influence of the TiO_2 nanorod content within P3HT:TiO_2 nanorod on the phase separation and photo-induced charge generation on surface by employing KPFM.

As the photovoltaic device architecture is considered, typically, the interlayer plays an important role for facilitating the collecting of the charges to electrodes. The functions of a TiO_2 nanorod layer incorporated on top of the hybrid surface within the structure are investigated by KPFM as well.

2. Experimental

The approach to synthesize the TiO_2 nanorod was according to the literature [14]. The as synthesized TiO_2 nanorod was capped by oleic acid. The surface of the TiO_2 nanorod was modified by pyridine treatment [13,15] following the approach in the literature. Films of blends of the P3HT:TiO_2 nanorod were prepared by spin coating on indium tin oxide (ITO)/poly (3,4-ethylenedioxythiophene)-poly (styrenesulfonate) (PEDOT:PSS) substrates following the approach in the literature [15]. To control good dispersion of the inorganic phase in the polymer, P3HT is dissolved in trichlorobenzene, and TiO_2 nanorods is dissolved in mixed solvent which contains pyridine, chloroform, and dichloromethane (1:3:2 by

* Corresponding author. Fax: +886 2 33664078.
E-mail address: suwf@ntu.edu.tw (W.-F. Su).

0009-2614/$ - see front matter © 2009 Elsevier B.V. All rights reserved.
doi:10.1016/j.cplett.2009.07.104

Author's personal copy

volume ratio). The thickness of the films was in the range of ~150 nm. For some of the samples, a pure TiO_2 nanorods layer (~20 nm) was cast on top of the hybrid from its pyridine solution acting as electron-collecting-hole-blocking layer [16]. The surface potential images were recorded using the KPFM (Veeco instruments Multimode AFM with an extender electronics module) operating in the lift mode (typical lift height 20 nm) by a silicon cantilevers with a PtIr surface coating in the dark or under white light illumination source (5 mW/cm^2). A Keithley Model 2410 source meter was used to supply voltage and measure current simultaneously.

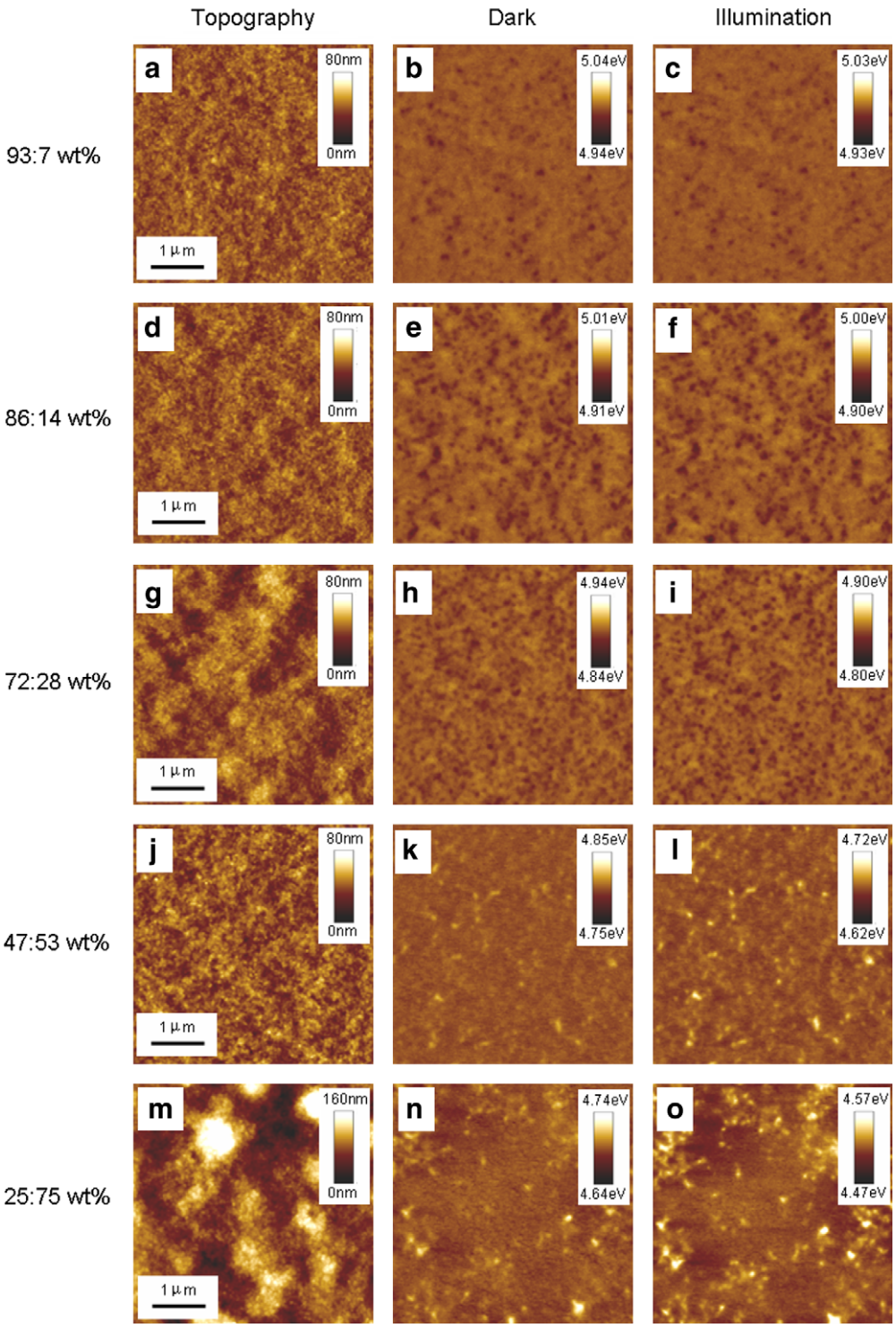

Fig. 1. Effects of hybrid composition on the topography and surface potential of the hybrids. Topographical images (a) and the corresponding surface potential images of P3HT:TiO_2 nanorod (93:7 wt.%) film on ITO/PEDOT:PSS in the dark (b) and under illumination (c). Topographical images (d) and the corresponding surface potential images of P3HT:TiO_2 nanorod (86:14 wt.%) film on ITO/PEDOT:PSS in the dark (e) and under illumination (f). Topographical images (g) and the corresponding surface potential images of P3HT:TiO_2 nanorod (72:28 wt.%) film on ITO/PEDOT:PSS in the dark (h) and under illumination (i). Topographical images (j) and the corresponding surface potential images of P3HT:TiO_2 nanorod (47:53 wt.%) film on ITO/PEDOT:PSS in the dark (k) and under illumination (l). Topographical images (m) and the corresponding surface potential images of P3HT:TiO_2 nanorod (25:75 wt.%) film on ITO/PEDOT:PSS in the dark (n) and under illumination (o).

Author's personal copy

3. Results and discussion

Fig. 1a displays the surface topographic image of the thin film of blended P3HT:TiO_2 nanorod (93:7 wt.%) spin-coated on ITO/PEDOT:PSS. Fig. 1b and c shows the corresponding surface potential image of the hybrid in dark and under illumination, respectively. The surface potential image in dark has been found separated into darker and brighter regions. The contrast in dark is explained due to the differences in the alignment of the energy levels of the domains of respective donor (P3HT) rich and acceptor (TiO_2) rich materials with the Fermi level of the bottom electrode [11]. Between regions with dissimilar compositions of hybrid, the contrast of the surface potential is shown due to the different energetic after the Fermi level alignment.

Upon illumination, the photo-generated excitons diffuse within P3HT and charge separation occurs at the P3HT:TiO_2 nanorod hetero-interface. The contrast is enhanced within surface potential image showing the tendency for the acceptor to capture the generated electron, and the donor to become comparatively positively charged; due to the larger electron affinity of TiO_2 nanorod can induce an electron transfer from P3HT to TiO_2. The darker regions with smaller surface potential are interpreted as the TiO_2 rich regions due to enriched with electron comparatively. The domains within surface potential images also reveal the continuity and interfaces of the defined hetero-structure of respective TiO_2 nanorod rich (darker) and P3HT rich (brighter) regions that are formed as a result of phase separation during film formation.

We explorer the role of the ratio of P3HT with respect to TiO_2 for forming available interfaces and the interpenetrating network for charge exciton dissociation and transport. The KPFM study for the evolution of topography and surface potential P3HT:TiO_2 nanorod films for five different concentration of TiO_2 is shown in Fig. 1. For the topography, the blends with low amounts of TiO_2 nanorod typically show a smooth surface. However, increasing the TiO_2 content to 75 wt.% results in coagulation, the growth of spherelike structure, and the significantly increased in surface roughness and surface height difference, which is attributed to the aggregation of the nanorods.

The surface potential images reveal the TiO_2 nanorod rich region barely occupying on surface with low TiO_2 loadings. As the loading of TiO_2 nanorod is increased, the increase in the hetero-interface of P3HT rich/TiO_2 rich domains is obtained. The connectivity of the TiO_2 rich phases is improved as shown in the potential image; result in percolated pathway for transport of electron to the electrode. With TiO_2 content up to 53 wt.%, the increase of TiO_2 nanorod rich region gradually approaches a uniformly P3HT:TiO_2 nanorod complex, thus providing a large and distributed interface area for photo-induced charge transfer. With the TiO_2 content increased to 75 wt.%, the presence of hole accumulation domains on surface are resolved within the potential images. This morphological feature may lead to shunt in a photovoltaic device with Al electron collecting electrode.

The potential contrast between domains is enhanced in the presence of illumination, reflecting the differences in the accumulation of photo-induced charges between nanophases of several tens of nanometer. The surface potential is negatively shifted as compared to in dark for these samples due to an excess of free photo-generated electrons present on surface. Shifting to a lower work function corresponds to an increase of electron density as compared to hole density, which is resulted from the built up of internal electric field, driving the electrons moving to the surface and the holes drifting to the underlying substrates [6]. As the shift in potential under irradiation for each of the five blends are compared, the negatively shift of potential is significant with high TiO_2 loading, reflecting an increasing of excess negative charge on surface due to improvement in charge separation and transport. The finer scale of phase separation is responsible for the higher numbers of photo-induced charges due to the shorter diffusion length for the exciton with higher TiO_2 loading. The charge generation is believed not only occurred at the interfaces between the nanodomains but also within the finer scale of phase separation.

We study the effect of TiO_2 loading on the charge transport within the hybrid. Space-charge-limited current (SCLC) method was used to determine electron mobility (μ_e) of the hybrid by using the Al/hybrid/Al configuration. The measured SCL electron and hole-only current using the corresponding device structures can be expressed by [17]

$$J_{e(h)} = \frac{9}{8} k\varepsilon_0 \mu_{e(h)} \frac{V^2}{L^3}$$

where $J_{e(h)}$, k, ε_0, V, and L are the electron (hole) current density, relative permittivity of the material, the permittivity of free space, effective voltage drop across the active material, and the thickness of the active material, respectively. As shown in Fig. 2, the electron mobility of the P3HT:TiO_2 nanorod hybrid increases with the increase of the TiO_2 nanorod loading. This has been attributed to the improvement in the quality of TiO_2 nanorod percolated paths which is consistent with the better connectivity of the TiO_2 rich domains mapped by KPFM under higher TiO_2 content.

Effects of TiO_2 nanorod top layer on the topography and surface potential of the hybrid are studied. We expect the TiO_2 nanorod layer will selectively collect the electron but block the hole present on the surface, as a pristine TiO_2 nanorod layer is deposited on the surface of ITO/PEDOT:PSS/P3HT:TiO_2 nanorod. The results of KPFM study of the P3HT:TiO_2 nanorod hybrid (47:53 wt.%) with TiO_2 nanorod top layer are shown in Fig. 3a–c for topography, potential in dark and illumination, respectively. We compare morphology and surface potential difference between the hybrid with and without TiO_2 nanorod top layer (Fig. 1j, k and l). The former shows a rougher topography, a lower surface contrast in dark and a large uniform negative shift in surface potential upon illumination. The results are expected because the KPFM probes the TiO_2 nanorod top layer without sensing much of the hybrid layer. The TiO_2 nanorod top layer is indeed function as an electron transport layer to enhance the electron collection.

The KPFM is also used for the study of the evolution of the change of surface potential upon illumination for P3HT:TiO_2 nanorod films for different concentrations with additional TiO_2 nanorod layer on surface. The results of negative shift of potential for both sets of hybrid with and without TiO_2 nanorod layer are illustrated in Fig. 4 (with TiO_2 nanorod = 0, 7, 14, 28, 53, 75 wt.% in hybrid

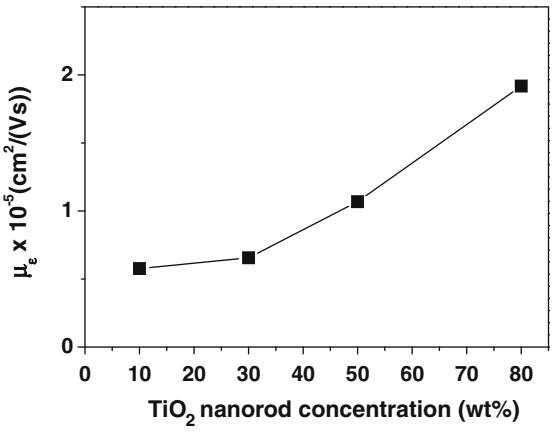

Fig. 2. Electron mobility for various TiO_2 nanorod loadings in the hybrid obtained from space-charge-limited-current (SCLC) measurements.

Author's personal copy

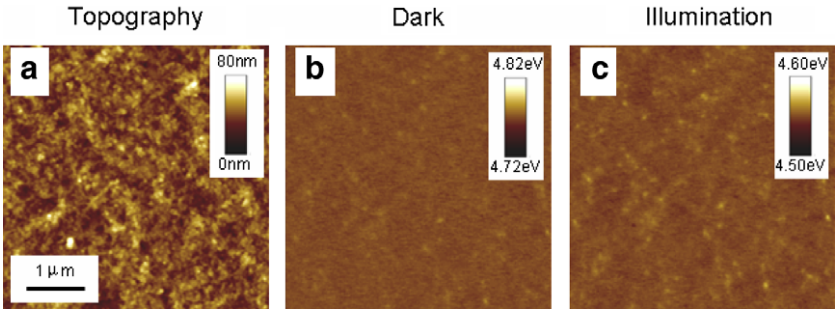

Fig. 3. Effects of TiO_2 nanorod top layer on the topography and surface potential of the hybrid, (a) topographical image, (b) the corresponding surface potential image in the dark (c) the corresponding surface potential image under illumination of ITO/PEDOT:PSS/P3HT:TiO_2 nanorod (47:53 wt.%)/TiO_2 nanorod configuration.

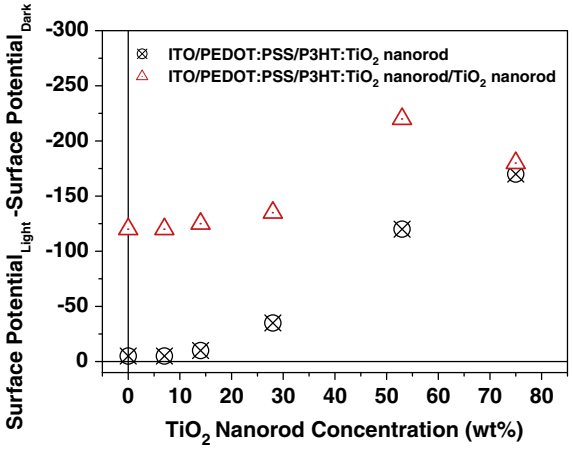

Fig. 4. The shift of average surface potential under illumination for ITO/PEDOT:PSS/P3HT:TiO_2 nanorod and ITO/PEDOT:PSS/P3HT:TiO_2 nanorod/TiO_2 nanorod as a function of concentration of TiO_2 nanorod in the blend.

P3HT:TiO_2 nanorod). For the result of the potential shift of devices under irradiation without nanorod layer, not much negative charge can be extracted from the hybrid at low loadings, this is due to the limited interfacial area and less connected percolation path. With incorporation of the TiO_2 nanorod layer, the uniformity of potential distribution is increased and shift of potential under irradiation is significantly raised caused by the additional hetero-interface on top of the hybrid that selectively collects the electron but blocks the hole. Upon illumination, the shift of potential is increased more significantly with the TiO_2 top layer than without the layer, within the hybrids with various TiO_2 loadings (with TiO_2 nanorod = 0, 7, 14, 28, 53 wt.%), except for the TiO_2 loading of 75 wt.%. Due to the large roughness and large height difference of the topography of the hybrid, forming a thin and conformal TiO_2 nanorod layer on the surface is more difficult. Thus the function of the this electron-transporting-hole-blocking layer is not significant in this case, as we compare the photo-response of potential between the structure of ITO/PEDOT:PSS/P3HT:TiO_2 nanorod (25:75 wt.%) with and without a TiO_2 nanorod layer (Fig. 4). The obtained KPFM result for the device architecture provides an explanation for the dependence of solar cell performance on TiO_2 nanorod loading in Ref. [13].

4. Conclusion

The KPFM is employed to resolve the topography as well as the presence of hetero-interfaces and charge percolation paths within the mixtures of P3HT and TiO_2 nanorods in the scale of tens of nanometer. Additionally, the KPFM is applied to map the photo-response of the hybrid of respective donor–acceptor materials. The correlation between the hybrid nano-scale structures with films' electronic properties is present. In addition, the KPFM is exploited to investigate the role played by the additional TiO_2 nanorod top layer within the structure. Finer scale of phase separation, enhanced electron transport and improved photo-induced electron extraction on surface are obtained for the hybrid with high TiO_2 loading. The TiO_2 nanorod layer deposited on top the hybrid can selectively collect the electron but block the hole. The obtained results offer a deeper insight into the correlation among the fabrication parameters of the polymer:inorganic nanocrystals' hybrid, structure of the photovoltaic device and the photovoltaic device conversion efficiency.

Acknowledgments

The authors thank the National Science Council of Republic of China (NSC 95-3114-P-002-003-MY3, 97-2623-7-002-009-ET) and the US Air Force Office of Scientific Research (AOARD-07-4014) for financial support of this research.

References

[1] W.U. Huynh, J.J. Dittmer, A.P. Alivisatos, Science 29 (2002) 2425.
[2] W.J.E. Beek, M.M. Wienk, M. Kemerink, X. Yang, R.A.J. Janssen, J. Phys. Chem. B 109 (2005) 9505.
[3] Y.-Y. Lin et al., J. Am. Chem. Soc. 131 (2009) 3644.
[4] I. Gur, N.A. Fromer, C.-P. Chen, A.G. Kanaras, A.P. Alivisatos, Nano Lett. 7 (2007) 409.
[5] H. Hoppe, T. Glatzel, M. Niggemann, A. Hinsch, M.Ch. Lux-Steiner, N.S. Sariciftci, Nano Lett. 5 (2005) 269.
[6] M. Chiesa, L. Bürgi, J.-S. Kim, R. Shikler, R.H. Friend, H. Sirringhaus, Nano Lett. 5 (2005) 559.
[7] V. Palermo, G. Ridolfi, A.M. Talarico, L. Favaretto, G. Barbarella, N. Camaioni, P. Samorì, Adv. Funct. Mater. 17 (2007) 472.
[8] V. Palermo, M. Palma, P. Samorì, Adv. Mater. 18 (2006) 145.
[9] A. Liscio, G.D. Luca, F. Nolde, V. Palermo, K. Müllen, P. Samorì, J. Am. Chem. Soc. 130 (2008) 780.
[10] C. Yin, B. Pieper, B. Stiller, T. Kietzke, D. Neher, Appl. Phys. Lett. 90 (2007) 133502.
[11] K. Maturová, M. Kemerink, M.M. Wienk, D.S.H. Charrier, R.A.J. Janssen, Adv. Funct. Mater. 19 (2009) 1379.
[12] C.Y. Kwong, W.C.H. Choy, A.B. Djurisic, P.C. Chui, K.W. Cheng, W.K. Chan, Nanotechnology 15 (2004) 1156.
[13] C.-H. Chang, T.-K. Huang, Y.-T. Lin, Y.-Y. Lin, C.-W. Chen, T.-H. Chu, W.-F. Su, J. Mater. Chem. 18 (2008) 2201.
[14] P.D. Cozzoli, A. Kornowski, H. Weller, J. Am. Chem. Soc. 125 (2003) 14539.
[15] T.-W. Zeng, H.-H. Lo, C.-H. Chang, Y.-Y. Lin, C.-W. Chen, W.-F. Su, Sol. Energ. Mater. Sol. Cells 93 (2009) 952.
[16] T.-W. Zeng et al., Nanotechnology 17 (2006) 5387.
[17] P.N. Murgatroyd, J. Phys. D 3 (1970) 151.